Original Article

Mettl3 deficiency leads to the upregulation of Cav1.2 and increases arrhythmia susceptibility in mice

Ling Shi[1,†], Xuexin Jin[1,†], Zheng Li[1,†], Rui Gong[1], Yang Guo[1], Jiudong Ma[1], Yang Zhang[1], Benzhi Cai[1], Baofeng Yang[1,2], Dongmei Gong[1,*], and Zhenwei Pan[1,2,3,*]

[1]Department of Pharmacology (Key Laboratory of Cardiovascular Research, Ministry of Education) at College of Pharmacy, Harbin Medical University, Harbin 150086, China, [2]Research Unit of Noninfectious Chronic Diseases in Frigid Zone, Chinese Academy of Medical Sciences (2019RU070), Harbin 150086, China, and [3]Key Laboratory of Cell Transplantation, the First Affiliated Hospital, Harbin Medical University, Harbin 150086, China

[†]These authors contributed equally to this work.

*Correspondence address. Tel: +86-451-86671354; E-mail: 453009812@qq.com (D.G.) / panzw@ems.hrbmu.edu.cn (Z.P.)

Abstract

Methyltransferase-like 3 (Mettl3) is a component of methyltransferase complex that mediates m^{6}A modification of RNAs, and participates in multiple biological processes. However, the role of Mettl3 in cardiac electrophysiology remains unknown. This study aims to explore the ventricular arrhythmia susceptibility of Mettl3$^{+/-}$ mice and the underlying mechanisms. Mice were anesthetized with 2% avertin (0.1 mL/10 g body weight) for echocardiography and programmed electrical pacing. Whole-cell patch clamp technique was used to examine the electrophysiological property of cardiomyocytes. The expression of Cav1.2 was determined by qRT-PCR and western blot analysis. The m^{6}A medication of mRNA was examined by MeRIP-Seq and MeRIP-qPCR. No differences are found in the morphology and function of the hearts between Mettl3$^{+/-}$ mice and wild-type (WT) controls. The QT and QTc intervals of Mettl3$^{+/-}$ mice are significantly longer. High-frequency electrical stimulation showed that heterozygous knockout of Mettl3 increases ventricular arrhythmia susceptibility. The whole-cell patch-clamp recordings showed that the APD is prolonged in Mettl3$^{+/-}$ ventricular myocytes and more EADs were observed. The density of I_{Ca-L} is substantially increased in ventricular myocytes of Mettl3$^{+/-}$ mice. The pore-forming subunit of L-type calcium channel Cav1.2 is upregulated in Mettl3$^{+/-}$ mice, while the mRNA of its coding gene *CACNA1C* does not change. MeRIP-Seq and MeRIP-qPCR showed that the m^{6}A methylation of *CACNA1C* mRNA is decreased in cultured Mettl3-knockdown cardiomyocytes and Mettl3$^{+/-}$ hearts. Collectively, deficiency of Mettl3 increases ventricular arrhythmia susceptibility due to the upregulation of Cav1.2 by reducing m^{6}A modification on *CACNA1C* mRNA in mice. This study highlights the role of m^{6}A modification in the regulation of cardiac electrophysiology.

Key words Mettl3, m^{6}A modification, arrhythmia, L-type calcium channel

Introduction

N6-methyladenosine (m^{6}A) modification commonly occurrs in eukaryotic mRNAs, which regulates multiple RNA and protein processing events during mammalian development and disease processes [1]. The m^{6}A modification of RNAs is catalyzed by methyltransferases such as methyltransferase-like 3 (Mettl3), Mettl14 and WTAP, recognized by m^{6}A reader proteins YTHDF1-3, and erased by demethylases FTO and ALKBH5 [2]. m^{6}A modification modulates many biological processes such as cell proliferation and

apoptosis, stem cell differentiation and inflammatory response, and DNA damage response, by regulating mRNA splicing, mRNA stability and translation efficiency [3,4]. The modification of m^{6}A is closely related to many cardiovascular diseases such as hypertension, cardiac hypertrophy, and heart failure [5].

Mettl3 is the most important component of the methyltransferase complex that plays very important role in the regulation of gene expression. Mettl3 methylates mRNA, identifies methylated mRNA, enhances mRNA stability, and directly promotes mRNA translation.

For example, Mettl3 promotes m^6A methylation on hepatoma-derived growth factor (*HDGF*) mRNA, and the reader insulin-like growth factor 2 mRNA-binding protein 3 (IGF2BP3) directly binds to the m^6A site and enhances HDGF mRNA stability [6]. Mettl3 promotes yes association protein (*YAP*) mRNA translation by recruiting YTHDF1/3 and eukaryotic translation initiation factor 3 subunit b (eIF3b) into the translation initiation complex [7].

Mettl3 is a critical regulator of cardiac diseases. Dorn *et al.* [8] identified Mettl3-mediated methylation of mRNA on N6-adenosines as a dynamic modification that is enhanced in response to hypertrophic stimuli. In neonatal cardiomyocytes subjected to hypoxia/reoxygenation, upregulation of Mettl3 decreases autophagic flux and promotes cell apoptosis, whereas knockout of Mettl3 enhances cell viability [9]. Li *et al.* [10] showed that forced expression of Mettl3 activates cardiac fibroblasts proliferation and fetal bovine serum, and promotes collagen production and deposition, while suppression of Mettl3 expression alleviates cardiac fibrosis and improves cardiac function in myocardial infarction mice. However, the role of Mettl3-mediated m^6A modification in cardiac electrophysiology remains unclear.

In the current study, we found that heterozygous knockout of Mettl3 increases ventricular arrhythmia susceptibility in mice, prolongs APD and upregulates I_{Ca-L} current and Cav1.2 expression.

Materials and Methods
Animal studies
Adult conventional Mettl3-knockout heterozygous mice (Mettl3$^{+/-}$ mice, 8–10 weeks old) were used in the study. Sex- and age-matched wild-type (WT) mice were used as controls. All mice are C57BL6 genetic background. The mice were kept in animal rooms with controlled temperature (22–25°C). Use of animals was approved by the Ethic Committees of Harbin Medical University (IRB3001719) and conformed to the Guide for the Care and Use of Laboratory Animals published by the US National Institutes of Health (NIH Publication No. 85-23, revised 1996).

Cardiac echocardiography
Mice were anesthetized with 2% avertin (0.1 mL/10 g body weight) for echocardiography. Both two-dimensional M-mode and three-dimensional Doppler echocardiography were performed by using the VINNO 6 imaging system (VINNO, Suzhou, China) to evaluate cardiac diameter and function. Derived echocardiography parameters including left ventricular ejection fraction (LVEF), left ventricular fractional shortening (LVFS), left ventricular posterior wall thickness at systolic phase (LVPWs) and left ventricular posterior wall thickness at diastolic phase (LVPWd), left ventricular internal dimension systole (LVIDs), left ventricular internal dimension diastole (LVIDd), interventricular septal thickness at end-systole (IVSs) and interventricular septal thickness at end-diastole (IVSd) were obtained.

Histological analysis and Masson's trichrome staining
Mice were anesthetized with 2% avertin (0.1 mL/10 g body weight) before heart dissection. Euthanasia was performed by cervical dislocation in anesthesia. Hearts were excised and fixed in 4% paraformaldehyde overnight, and then embedded in paraffin. The preparations were cut vertical-sectionally into 5-μm-thick sections. Haematoxylin and eosin (HE) and Masson's trichrome staining were performed and the stained sections were examined and pictured

with Leica Aperio Versa 8 (Leica, Nussloch, Germany) microscope. The HE staining images were analyzed with ImageScope x64 to quantify the morphology of hearts. The percentage of fibrotic tissue was determined by measuring collagen deposition on Masson's trichrome-stained sections using Image-Pro Plus 6.0.

Mouse electrocardiography
Electrocardiographs (ECGs) were obtained from mice at rest and under stress as reported previously [11]. Briefly, after mice were anesthetized with avertin (0.1 mL/10 g body weight), anesthetized WT and Mettl3$^{+/-}$ mice were placed on a heating pad (28°C) and subcutaneous needle electrodes were applied to the left, right upper limb and right lower limb for ECG recording. The ECG waveforms were continuously monitored under anesthesia until heart rate stabilized. Baseline ECG was recorded for 5 min, followed by the intraperitoneal injection of epinephrine (1.6 mg/kg) and caffeine (120 mg/kg). ECG was then continuously recorded for another 30 min. ECG traces were analyzed using the BL-420 biological signal acquisition system (Chengdu Techman Software Co.LTD, Chengdu, China).

Electrophysiological study *in vivo*
Electrophysiological study was performed according to protocols reported previously [12–14]. Mice were anesthetized with 2% avertin. An octapolar electrophysiological catheter (1.1 F; SciSense Inc, Ontario, Canada) was inserted into the jugular vein and advanced to the right atrium or right ventricular for intracardiac pacing experiments using an automated stimulator interfaced with the data acquisition system (GY6000; HeNanHuaNan Medical Science & Technology Ltd, Zhengzhou, China). To determine VERP, the single ventricular extra stimulus was placed at a pacing drive of 100 ms. A drive train of eight paced beats (S1 × 8) followed by delivery of a single extra stimulus (S2) was given. The extra stimulus was decremented in 2 ms intervals until refractoriness was reached. The pacing cycle length for the first 5-s burst was 40 ms, decreasing in each successive burst with a 2 ms decrement down to a cycle length of 20 ms to induce atrial arrhythmias. Successful induction of atrial fibrillation (AF) was defined as the occurrence of rapid irregular atrial rhythm lasting for 1 s or more. The AF episodes of atrial fibrillation is the number of atrial fibrillation that occurs during 11 episodes (the PCL decreased from 40 ms to 20 ms at 2 ms decrement interval) of rapid pacing in each mouse. The standard protocol of electrical stimulation for ventricular arrhythmia induction is: 10 basal stimuli (S1) followed by up to 2–3 extra stimuli (S2–S3), delivered with a coupling interval decreasing in steps of 2 ms until ventricular refractoriness was reached. The stimulation (S1) pattern was used and the whole stimulation process was repeated at 70 ms, 80 ms, and 90 ms cycle lengths, respectively. Occurrence and frequency of inducible arrhythmias were documented. More than three consecutive irregular fluctuations in the ventricle were considered to produce ventricular fibrillation.

Ventricular myocytes isolation
Mice were anesthetized with 2% avertin (0.1 mL/10 g body weight) and euthanized via cervical dislocation. Heart was rapidly removed and placed in Ca^{2+}-free Tyrode's solution consisting of 126 mM NaCl, 5.4 mM KCl, 0.33 mM NaH_2PO_4, 10 mM HEPES, 5.55 mM glucose, and 1 mM $MgCl_2$, with pH adjusted to 7.4 using NaOH. The heart was cannulated and perfused with calcium free Tyrode's so-

lution for 2–4 min, then switched to enzyme-containing solution (1 mg/mL collagenase type II, 1 mg/mL bovine serum albumin, and 0.1 ml/L of 0.9 M CaCl$_2$) on the Langendorff perfusing system. After digestion for 10–20 min, the ventricular was removed and agitated gently in Ca^{2+}-free Tyrode's solution that contains 0.5% bovine serum albumin. The solutions were warmed to 37°C and mixed with 95% oxygen and 5% carbon dioxide.

Whole-cell patch clamp recordings

Whole-cell patch clamp technique was used to record I_{to}, I_{k1}, I_{Ca-L} and action potentials of isolated ventricular myocytes at 37°C with an Axopatch 700B amplifier (Axon Instruments, Foster City, USA). Action potentials were elicited in current clamp mode by injection of brief current pulses (0.8–1 nA lasting 2 ms) at a stimulation frequency of 1 Hz. The recording electrodes (Borosilicate glass; Sutter Instrument, Novato, USA) were pulled (P-97; Sutter Instrument) and polished (F-83; Narishige, Tokyo, Japan) down to 2–3 MΩ when filled with pipette solution. The pipette solution for I_{to}, I_{k1} and action potentials recording contains: 130 mM K-glutamate, 1 mM MgCl$_2$, 15 mM KCl, 1 mM NaCl, 5 mM EGTA, 5 mM MgATP, 1 mM CaCl$_2$, and 10 mM HEPES, with pH adjusted to 7.2 using KOH, and the external solution was the Tyrode's solution containing 0.9 M CaCl$_2$. L-type Ca^{2+} current was elicited by depolarizing voltage steps between −60 and + 60 mV in 10 mV increments from a holding potential of −50 mV. The extracellular solution contains: 130 mM CsCl, 1 mM MgCl$_2$, 10 mM HEPES, 10 mM EGTA, 4 mM MgATP, and 0.1 mM NaGTP, with pH adjusted to 7.2 using CsOH. The pipette solution contains: 100 mM CsCl, 40 mM CsOH, 1 mM CaCl$_2$, 1 mM MgCl$_2$, 2 mM MgATP, 10 mM EGTA and 10 mM HEPES, with pH adjusted to 7.4 using CsOH.

Primary culture of neonatal mice cardiomyocytes and transfection

Cardiomyocytes were isolated from 1 to 3-day-old neonatal mice (C57BL/6) according to the procedures identical to those described in our previous study [15]. In brief, after dissection and washes, hearts were minced and the chunks were placed in 0.25% trypsin and digested for 3–4 h at 37°C. The combined cell suspension was centrifuged and resuspended in Dulbecco's modified Eagle's medium (DMEM) supplemented with 10% fetal bovine serum, 100 U/mL penicillin and 100 μg/mL streptomycin, and cultured in a culture flask at 37°C for 90 min. After fibroblasts preferentially adhered to the bottom, the on-adherent and weakly attached cells (mainly cardiomyocytes) were removed and seeded into culture plates. The cells were incubated at 37°C in a humidified atmosphere of 5% CO$_2$ and 95% air. After 48 h, cardiomyocytes that adhered onto the culture plates were used for subsequent experiments.

Mettl3-specific siRNA (siMettl3) or its negative control siRNA (NC) was mixed with Opti MEM® I Reduced Serum Medium (Gibco, New York, USA) for 5 min and then with X-treme GENE siRNA Transfection Reagent (#10810500; Roche, Basle, Switzerland) at room temperature. After 20 min of incubation, the siRNA was transfected into neonatal mice cardiomyocytes at a final concentration of 100 nM for Mettl3 knockdown. Forty-eight hours after transfection, cells were collected for western blot analysis, m^{6}A immunoprecipitation, and sequencing. The sequences of siMettl3 were: sense 5′-GCUACCGUAUGGGACAUUAUT-3′ and antisense 5′-UAAUGUCCCAUACGGUAGCTT-3′. The sequences of negative control (NC) siRNA were: sense 5′-GCGACGAUCUGCCUAAGAUTT-

3′ and antisense 5′-AUCUUAGGCAGAUCGUCGCTT-3′.

m^{6}A immunoprecipitation and sequencing

Total RNA was extracted from primary cardiomyocytes transfected with NC or Mettl3 siRNA. Total RNA (1–3 μg) was added to 300 μL 1 × IP buffer (50 mM Tris-HCl, pH7.4, 150 mM NaCl, 0.1% NP40, and 40 U/μL RNase inhibitor) containing 2 μg anti-m^{6}A rabbit polyclonal antibody (Synaptic Systems, Goettingen, Germany). The reaction mixture was incubated with head-over-tail rotation at 4°C for 2 h. Then, Dynabeads™ M-280 Sheep Anti-Rabbit IgG suspension (Invitrogen, Carlsbad, USA; 20 μL/sample) was blocked with freshly prepared 0.5% BSA at 4°C for 2 h, washed three times with 300 μL 1 × IP buffer, and resuspended in the total RNA-antibody mixture prepared above. The binding of RNAs to the m^{6}A-antibody beads were carried out with head-over-tail rotation at 4°C for 2 h. The beads were then washed three times with 500 μL 1 × IP buffer and twice with 500 μL Wash buffer. The enriched RNA was eluted with 200 μL Elution buffer at 50°C for 1 h. The RNA was extracted using acid phenol-chloroform and precipitated with ethanol. After labeling and hybridization, the hybridized arrays were washed, fixed and scanned using an Agilent Scanner G2505C (Agilent Technologies, Santa Clara, USA). Agilent Feature Extraction software (version 11.0.1.1) was used to analyze acquired array images.

Methylated RNA immunoprecipitation (MeRIP)

Ventricular tissues from WT and Mettl3$^{+/-}$ mice were subject to methylated RNA immunoprecipitation (MeRIP) assay using ribo-MeRIP™ m^{6}A Transcriptome Profiling Kit (R11096.3; RiboBio, Guangzhou, China) according to the manufacturer's recommendations. In short, 100 μg total RNA was isolated and randomly fragmented into 100 nucleotides or less, followed by the immunoprecipitation using 5 μg m^{6}A antibody which was linked to Magnetic Beads A/G. To determine the appropriate ratio between RNA and antibody, a dilution assay had been performed to optimize the MeRIP system and ensure the m^{6}A antibody was not saturated. One-tenth volume of fragmented RNA was saved as "10% input". Elution of m^{6}A-precipitated RNA was based on N6-methyladenosine 5′-monophosphate sodium salt. Modification of m^{6}A on *CACNA1C* mRNA was determined by qPCR analysis with forward primer: 5′-CCTGGAACGAGTGGAGTATC-3′ and reverse primer: 5′-CATTGCGGAGGTAAGCGTTG-3′.

Real-time RT-PCR

Total RNA was extracted from ventricular tissues using Trizol reagent (Invitrogen). Total RNA (0.5 μg) was reverse transcribed by using the TransScript reverse transcriptase (GMO Technology, Beijing, China) to obtain cDNA. The mRNA levels were determined using SYBR Green I incorporation method on ABI 7500 fast Real Time PCR system (Applied Biosystems, Foster City, USA). The relative expression level was calculated using the $2^{-\Delta\Delta CT}$ method and normalized to the level of *GAPDH* for each sample. The sequences of primers are listed in Table 1.

Western blot analysis

Total protein (60 μg) extracted from ventricular tissues was fractionated by SDS-PAGE (8% polyacrylamide gels) and transferred onto nitrocellulose membrane. The membrane was blocked with 5% nonfat milk for 1.5 h at room temperature. The membrane was then incubated with primary antibodies against the following pro-

Gene	Sequences of primers
Mus *Mettl3*	Forward 5′-AACTTACGCTGACCACTCCA-3′
	Reverse 5′-CCAGACCAGATGCTAAAGAG-3′
Mus *CACNA1C*	Forward 5′-CTTACGCTGCGGGTCTCATCT-3′
	Reverse 5′-TACTCATCCACGGGCTCCAAT-3′
Mus *KCND2*	Forward 5′-GGCAGTGTGCAAGAACTCAG-3′
	Reverse 5′-GCTGTGGTCACGTAAGGTTG-3′
Mus *KCNJ2*	Forward 5′-AACCGCTACAGCATCGTCTC-3′
	Reverse 5′-TCTTGCCATTCCCAAAGCCA-3′
Mus *GAPDH*	Forward 5′-AAGAAGGTGGTGAAGCAGGC-3′
	Reverse 5′-TCCACCACCCAGTTGCTGTA-3′

teins: Mettl3 (1:500 dilution; Proteintech, Rosemont, USA), CAC-NA1C (1:1000 dilution; Abcam; Cambridge, UK), KCND2 (1:200 dilution; Alomone Labs, Jerusalem, Israel), KCNJ2 (1:200 dilution; Alomone Labs) and GAPDH (1:10000 dilution; Absin Bioscience, Shanghai, China) on a shaking bed overnight at 4°C. The membrane was washed with PBS-T for three times and incubated with rabbit secondary antibodies (1:10000; Abcam) at room temperature for 1 h. Finally, the membrane was rinsed with PBS-T before scanned with an Imaging System (LI-COR Biosciences, Lincoln, USA).

Statistical analysis

Data were presented as the mean ± SEM. Statistical analysis was performed using unpaired Student's *t*-test between two groups, and one-way ANOVA followed by post-hoc Tukey's test was used for multiple group comparisons. The difference was considered significant when $P < 0.05$.

Results

The cardiac morphology and function of Mettl3$^{+/-}$ mice

As conventional homozygous knockout of Mettl3 leads to embryonic lethality in mice, we employed the heterozygous Mettl3-knockout (Mettl3$^{+/-}$) mice in the study. Firstly, we detected the mRNA and protein levels of Mettl3 in the hearts of heterozygotes mice and found that they were substantially reduced (Figure 1A,B). HE staining showed that the hearts from both WT and Mettl3$^{+/-}$ mice were not different in morphology (Figure 1C). There was no difference in heart-to-body weight ratio or lung-to-body weight ratio between WT and Mettl3$^{+/-}$ mice (Figure 1D,E). Masson's trichrome staining showed that no fibrosis was detected in the ventricular tissue of Mettl3$^{+/-}$ mice (Figure 1F,G). The echocardiographic examination showed that Mettl3 deficiency did not affect ejection fraction (EF), fractional shortening (FS), left ventricular posterior wall thickness (LVPW), left ventricular internal dimension (LVID) or interventricular septal thickness (IVS) in mice (Figure 1H–P). These data indicated that heterozygous ablation of Mettl3 does not produce morphological or functional changes in the hearts of mice.

Prolonged QT and QTc intervals and increased susceptibility to ventricular arrhythmia in Mettl3$^{+/-}$ mice

The ECG recordings showed that the heart rate (HR), RR intervals, P wave duration and PR intervals did not change in Mettl3$^{+/-}$ mice compared to those in WT mice (Figure 2A–E), which indicated that the electrophysiology of the sinoatrial node and atria were not affected. The QT intervals and heart rate-corrected QT interval (QTc) were significantly longer in Mettl3$^{+/-}$ mice than in WT mice (Figure 2F,G). The ventricular effective refractory period (VERP) was longer in Mettl3$^{+/-}$ mice than in WT mice (Figure 2H). The vulnerability to

arrhythmia of Mettl3$^{+/-}$ mice was then evaluated by programmed pacing. Both the ventricular fibrillation (VF) induction rate and the VF episodes were higher in Mettl3$^{+/-}$ mice than in WT mice (Figure 2I–K). Furthermore, the duration of the ventricular fibrillation in Mettl3$^{+/-}$ mice was longer than that in WT mice (Figure 2L). No significant change of atrial fibrillation (AF) susceptibility was observed in Mettl3$^{+/-}$ mice.

Mettl3$^{+/-}$ mice developed cardiac arrhythmias in response to sympathetic stress

In order to introduce interventions that more clearly produce real arrhythmic events, we performed the epinephrine/caffeine challenge as previously described [11]. Mettl3$^{+/-}$ mice demonstrated normal ECG recordings and regular heart rhythm at rest, similar to WT mice (Figure 3A,B, SR part). However, upon sympathetic stress through administration of epinephrine (1.6 mg/kg) and caffeine (120 mg/kg), Mettl3$^{+/-}$ mice more readily developed ventricular arrhythmias than WT mice, characterized by irregular heart rates, sustained ventricular arrhythmias episodes, premature ventricular contraction and polymorphic ventricular arrhythmias (Figure 3B). These data demonstrated that Mettl3 deficiency predisposes the heart to stress-induced ventricular arrhythmias.

Prolongation of action potentials and increased I_{Ca-L} currents in ventricular myocytes from Mettl3$^{+/-}$ mice

QT interval represents the average action potential duration of ventricular myocytes [16]. Therefore, action potentials were measured in isolated ventricular myocytes. The APD$_{50}$ and APD$_{90}$ were significantly longer in Mettl3$^{+/-}$ than those in WT myocytes (Figure 4A–C). There was no significant difference in resting membrane potentials, overshoot, threshold potentials and the maximum upstroke velocity (V_{max}) (Figure 4D–G). Consistent with the change in APD duration, 12 of 30 Mettl3$^{+/-}$ myocytes elicited frequent EADs, while only 3 of 30 WT myocytes exhibited occasional EADs (Figure 4H–J). The density of I_{Ca-L} of isolated ventricular myocytes was increased at indicated holding potentials in ventricular myocytes of Mettl3$^{+/-}$ mice compared to that in WT controls, with a peak increase of 64% at the voltage of 0 mV (maximum I_{Ca-L}: WT 9.81 ± 1.02 pA/pF vs Mettl3$^{+/-}$ 16.11 ± 1.35 pA/pF) (Figure 4K,L). The voltage-dependent I_{Ca-L} activation and voltage for the half-maximal activation ($V_{1/2}$) were not different between the two groups (Figure 4M,N). In line with the increase of I_{Ca-L} in Mettl3$^{+/-}$ mice, the protein level of Cav1.2 was increased, while the mRNA level of CACNA1C did not change (Figure 4O,P).

Mettl3 deficiency did not change I_{k1} or I_{to} current

We next performed voltage-clamp experiments to record inward rectifier potassium current (I_{k1}), transient outward potassium current (I_{to}) and steady-state potassium current (I_{ss}). The densities of I_{k1}, I_{to} and I_{ss} showed no significant difference in ventricular myocytes from WT and Mettl3$^{+/-}$ mice (Figure 5A–E). The protein and mRNA levels of Kv4.2 and Kir2.1 did not change (Figure 5F–I).

Increase of I_{Ca-L} and upregulation of Cav1.2 in neonatal cardiomyocytes transfected with Mettl3 siRNA

Subsequently, we recorded the I_{Ca-L} and detected the protein level of Cav1.2 in neonatal cardiomyocytes transfected with Mettl3 siRNA. The Mettl3 siRNA (siMettl3) produced approximately 50% reduction of Mettl3 mRNA and protein levels (Figure 6A,B). The I_{Ca-L} was

increased in neonatal cardiomyocytes from transfected of siMettl3 compared to that in NC controls, with a maximum of 69% at the voltage of 0 mV (maximum I_{Ca-L}: NC 3.64 ± 0.33 pA/pF vs siMettl3 6.18 ± 0.89 pA/pF) (Figure 6C,D), while the voltage-dependent I_{Ca-L} activation and $V_{1/2}$ were not different (Figure 6E,F). The protein level of Cav1.2 was upregulated after Mettl3 knockdown (Figure 6G).

Decrease of *CACNA1* m⁶A modification after Mettl3 deficiency

To assess a possible role of m⁶A modifications on mRNA in cardiomyocytes transfected with Mettl3 siRNA, we performed an independent m⁶A quantification experiment to assess if the overall percentage of m⁶A in RNA changes after transfection with Mettl3 siRNA. We isolated RNA from neonatal mice cardiomyocytes. By using an antibody-mediated capture of m⁶A followed by colorimetric analysis, we found that the percentage of m⁶A RNA modification was decreased substantially after transfection with Mettl3

siRNA (Figure 7A). To investigate how Mettl3 deficiency influences the expression of Cav1.2, we examined the m⁶A modification of *CACNA1C* mRNA. The m⁶A-mRNA epitranscriptomic microarray on primary cardiomyocytes showed that the m⁶A modification of *CACNA1C* mRNA was downregulated after Mettl3 was knocked down (Figure 7B). Furthermore, the MeRIP-qPCR assay was conducted to determine the enrichment of m⁶A on the *CACNA1C* mRNA in the hearts of WT and Mettl3⁺/⁻ mice. It was found that the amount of *CACNA1C* modified by m⁶A was remarkably decreased in the hearts of Mettl3⁺/⁻ mice compared to that in the WT mice (Figure 7C). These results suggested that m⁶A modification of *CACNA1C* mRNA was influenced by Mettl3.

Discussion

Mettl3 acts as the catalytic subunit of the m⁶A methyltransferase complex and is responsible for installing the m⁶A modification on mRNA. Perturbations in m⁶A level due to the depletion or overexpression of Mettl3 can lead to cardiac diseases, such as hyper-
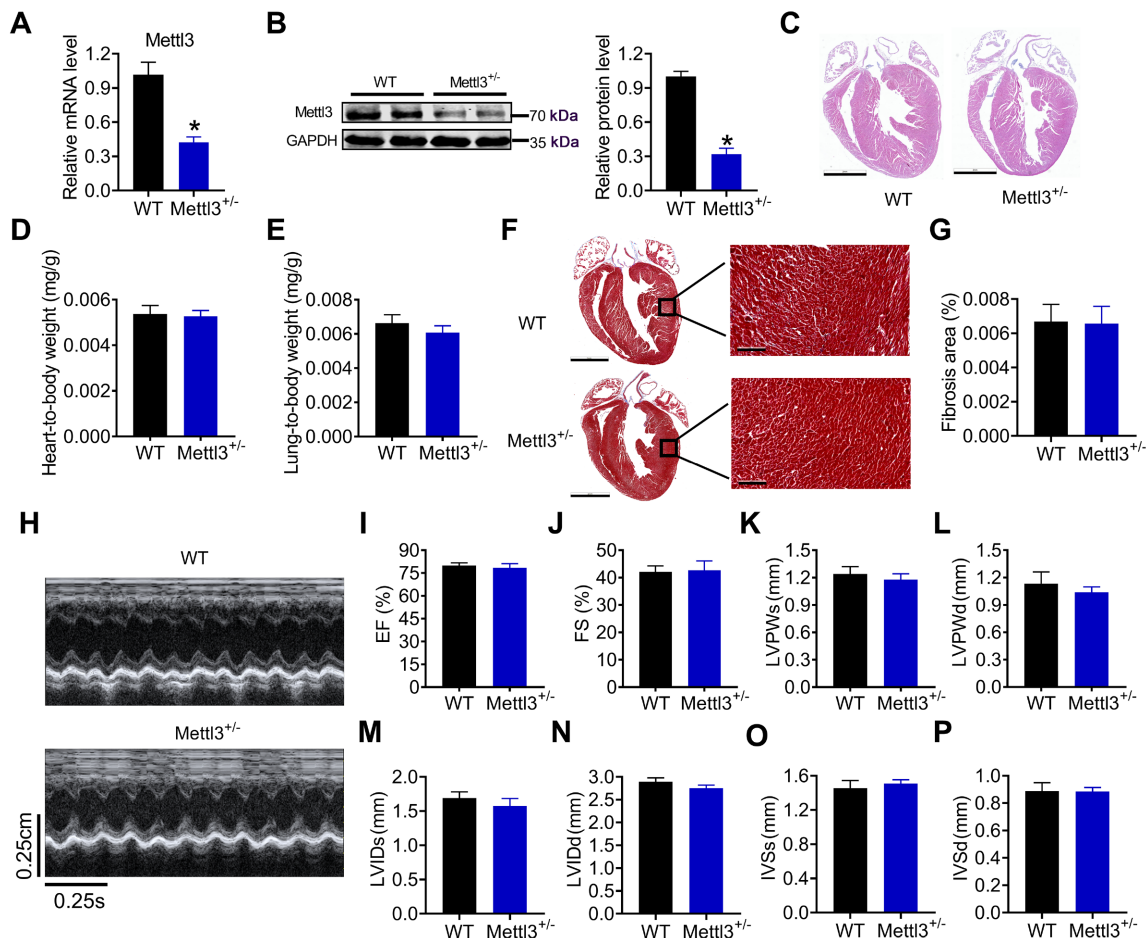
Figure 1. The cardiac morphology and function of Mettl3⁺/⁻ mice (A,B) Verification of Mettl3 down-regulation at both mRNA and protein levels in WT and conventional Mettl3 knockout heterozygotes mice (Mettl3⁺/⁻ mice) (n = 3). (C) Representative HE stained paraffin section display morphology of WT and Mettl3⁺/⁻ hearts, showing the similar cardiac dilation and wall thickness (n = 5). Scale bar: 2 mm. (D) Heart-to-body weight ratios of WT and Mettl3⁺/⁻ hearts (n = 10). (E) Lung-to-body weight ratios of WT and Mettl3⁺/⁻ mice hearts (n = 10). (F) Representative Masson's Trichrome staining of WT and Mettl3⁺/⁻ mice hearts (n = 5). Scale bar: 2 mm (whole heart) and 100 μm (enlarged part). (G) The quantification of the total fibrotic area using Image-Pro Plus (n = 5). (H) Representative cardiac echocardiographic pictures of WT and Mettl3⁺/⁻ mice. (I–P) Ejection fraction (EF), fractional shortening (FS), left ventricular posterior wall thickness at systolic phase (LVPWs), left ventricular posterior wall thickness at diastolic phase (LVPWd), left ventricular internal dimension systole (LVIDs), left ventricular internal dimension diastole (LVIDd), interventricular septal thickness at end-systole (IVSs) and interventricular septal thickness at end-diastole (IVSd) of hearts by echocardiography. n = 10. Data are expressed as the mean ± SEM. *$P < 0.05$ vs WT by t-tests.
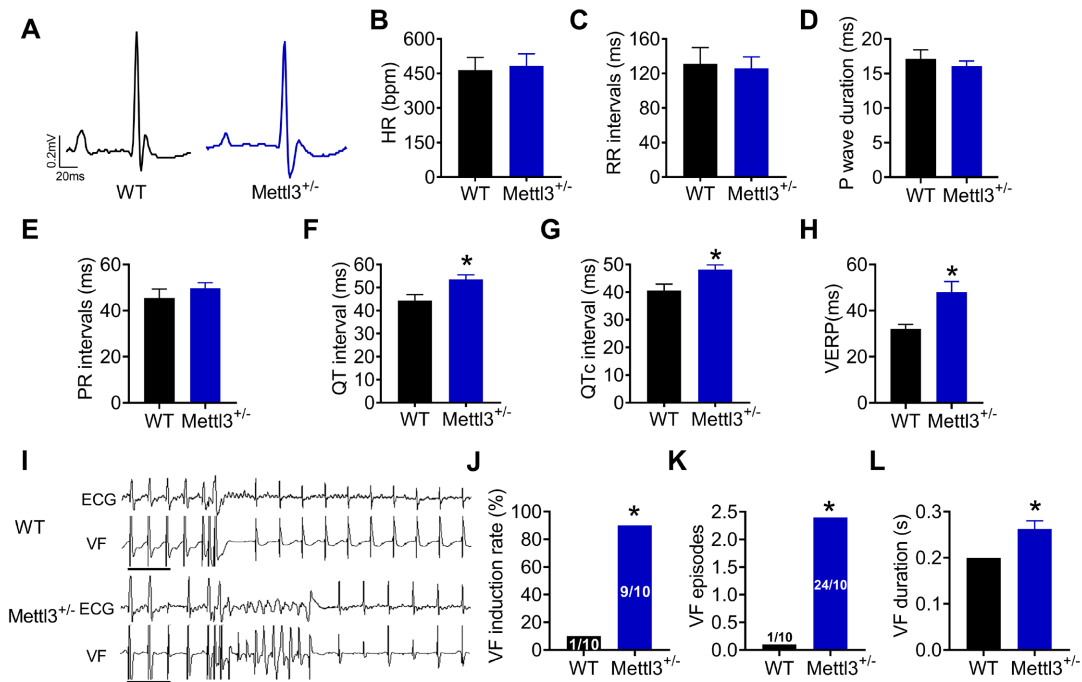
Figure 2. Prolonged QT and QTc intervals and increased susceptibility to ventricular arrhythmia of Mettl3+/− mice (A) Examples of surface ECGs recorded from WT controls and Mettl3+/− mice. (B) Heart rates. (C) RR intervals. (D) P wave uration. (E) PR intervals. (F) QT interval. (G) The corrected QT intervals (QTc). (H) The ventricular effective refractory period (VERP) of WT controls and Mettl3+/− mice. (I) Representative traces of pacing induced ventricular fibrillation (VF). Scale bar: 200 ms. (J) Induction rate of VF. (K) VF episodes. (L) VF duration. n = 10. Data are expressed as the mean ± SEM. *$P < 0.05$ vs WT by t-tests.
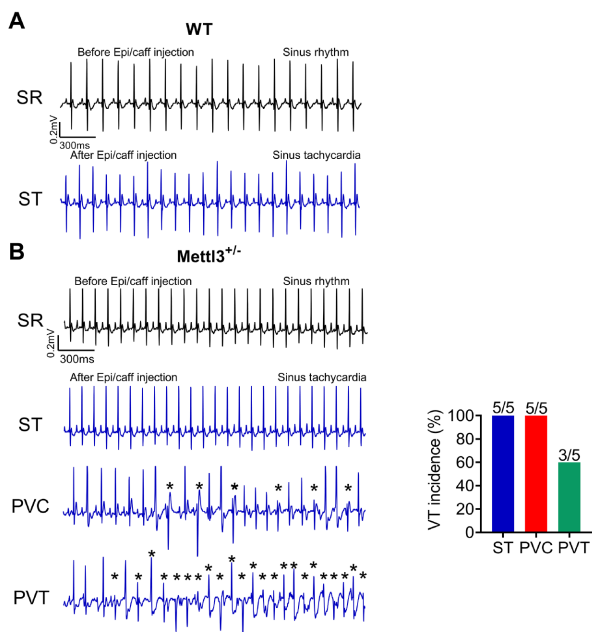
Figure 3. Mettl3+/− mice developed cardiac arrhythmias in response to sympathetic stress (A,B) Representative ECG recordings from WT and Mettl3+/− mice before and 5–15 min after intraperitoneal injection of epi/caff (*Arrhythmia onset). The histogram shows the incidence of different types of VT (ST, PVC and PVT) calculated from Mettl3+/− mice in response to epi/caff. n = 5. epi/caff: epinephrine (1.6 mg/kg) and caffeine (120 mg/kg). SR: Sinus rhythm; ST: Sinus tachycardia; PVC: Premature ventricular contraction; PVT: Polymorphic ventricular tachycardia.

trophy, heart failure and ischemia [4]. In this study, we discovered that heterozygous knockout of Mettl3 in mice increases the occurrence of ventricular arrhythmia, which implies that m6A modification may participate in cardiac arrhythmogenesis.

The alteration of action potential duration (APD) is the major cause of arrhythmia. Action potential prolongation provides a substrate for early after-depolarizations (EADs), and EADs are triggers of cardiac arrhythmias [17]. In this study, we recorded the APD of Mettl3+/− mice and found that Mettl3+/− mice had prolonged APD and were more prone to trigger EADs. The APD and its wave form were determined by measuring the activity of several transmembrane ionic currents in cardiomyocytes. The voltage-gated L-type calcium channel is the main pathway for Ca^{2+} influx into excitable cells in response to the membrane depolarization [18], which forms one part of cardiomyocyte action potentials. Abnormal calcium homeostasis may increase the occurrence of EADs and delayed after-depolarizations (DADs) that finally contribute to ventricular arrhythmia [19]. In this study, we found that I_{Ca-L} was significantly up-regulated in the ventricular myocytes of Mettl3+/− mice relative to that of WT mice; meanwhile, APD was remarkably prolonged. Consistently, the protein level of Cav1.2 was increased in the hearts of Mettl3+/− mice compared to that in the WT mice, while the mRNA of *CACNA1C* did not change. I_{to} and I_{k1} also play a key role in the formation of APD. I_{to} is important for the early repolarization in the ventricular action potential, and downregulation of I_{to} may contribute to APD prolongation [20]. Reductions in I_{k1} may contribute to reduced repolarization reserve, ventricular APD prolongation, and may increase risk for DAD-induced ventricular arrhythmias [21]. Our data suggested that I_{to} and I_{k1} did not change in Mettl3+/− ventricular myocytes.
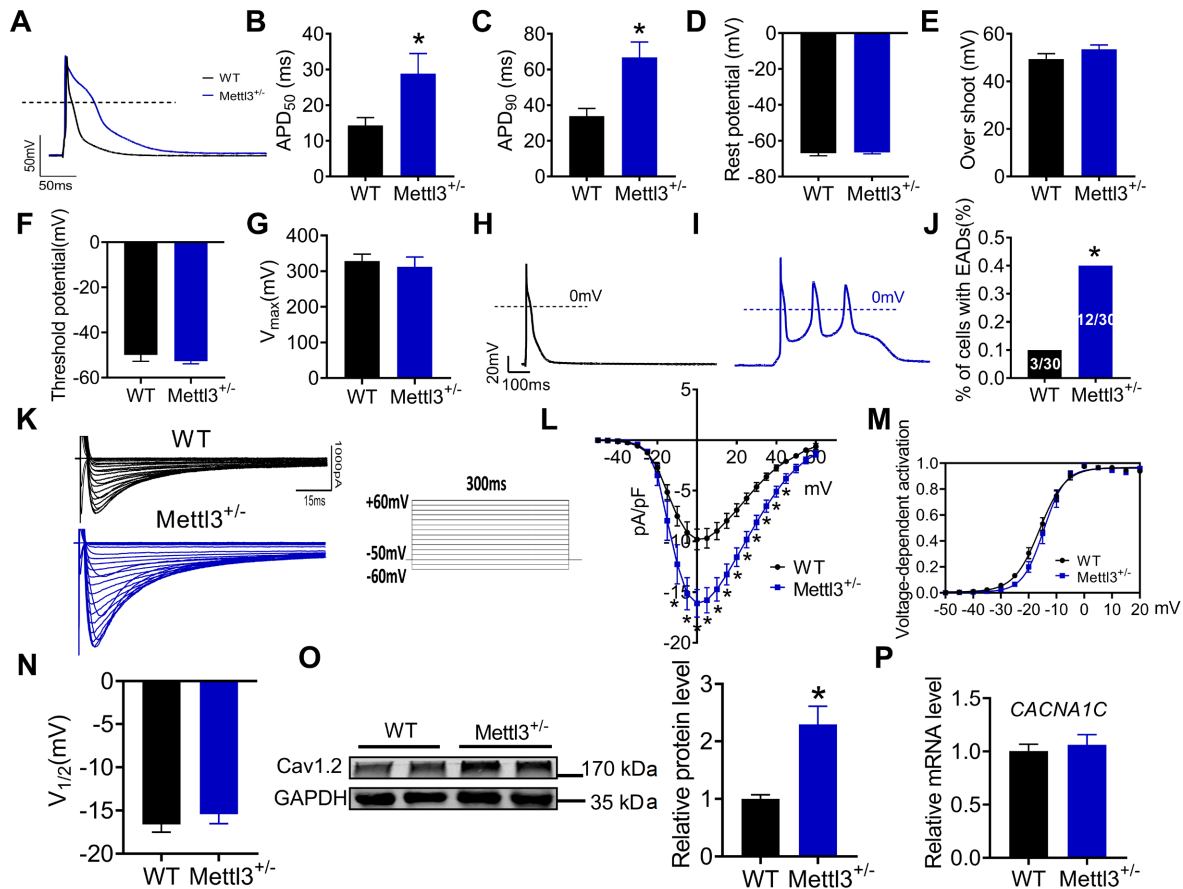
Figure 4. Prolongation of action potentials and increased I_{Ca-L} currents in ventricular myocytes from Mettl3$^{+/−}$ mice (A) Representative traces of APD of single ventricular myocytes by patch-clamp technique. (B,C) Statistical analysis of APD$_{50}$ and APD$_{90}$ from single ventricular myocytes. (D–G) Statistical analysis of rest potential, overshoot, threshold potential and the maximum upstroke velocity (Vmax) of ventricular myocytes (n = 15–20 cells). (H) Representative traces of AP of single WT ventricular myocytes by patch-clamp technique. (I) Representative traces of EAD of single Mettl3$^{+/−}$ ventricular myocytes. (J) The percentage of cells with EADs (n = 30 cells). (K) Representative traces of I_{Ca-L} in WT and Mettl3$^{+/−}$ ventricular myocytes. (L) Statistical analysis of the current density of I_{Ca-L} (n = 12–15 cells). (M) Voltage-dependent I_{Ca-L} activation (n = 12–15 cells). (N) Voltage for the half-maximal activation V$_{1/2}$ (n = 12–15 cells). (O) Protein expression of Cav1.2 in WT and Mettl3$^{+/−}$ mice hearts. (P) mRNA expression of CACNA1C in WT and Metttl3$^{+/−}$ mice hearts. N = 3. Data are expressed as the mean ± SEM. *$P < 0.05$ vs WT by t-tests.

Previous studies showed that m^{6}A RNA modification regulates gene expression post-transcriptionally in multiple cell types [22,23]. Enrichment of m^{6}A near the exons and stop codon regions has been shown to regulate translation [24]. Indeed, studies have shown that alteration of m^{6}A modification affects the translation of specific mRNAs [25]. m^{6}A modification can regulate RNA stability and translation efficiency in myocytes [26,27]. To determine the role of m^{6}A methylation in the heart, we isolated primary cardiomyocytes transfected with NC or Mettl3 siRNA, and performed m^{6}A immunoprecipitation followed by RNA sequencing. Our results showed that the level of m^{6}A modification of CACNA1C mRNA was reduced after knockdown of Mettl3. As the mRNA level of CACNA1C did not change in the heats of Mettl3$^{+/−}$ mice, while Cav1.2 level was upregulated, we speculate that changes in m^{6}A RNA methylation of CACNA1C mRNA may enhance the protein translation of Cav1.2.

As reported in previous studies, Mettl3 was closely related to cardiac hypertrophy [8,28], while the data were contradictory. Dorn et al. [8] demonstrated that overexpression of Mettl3 in mice led to cardiac hypertrophy, whereas knockdown of Mettl3 developed

cardiomyocyte remodeling and dysfunction, which emphasized the importance of this new stress-response mechanism in the heart for maintaining normal cardiac function. However, Kmietczyk et al. [28] showed that cardiac-specific overexpression of Mettl3 attenuated pathological hypertrophic cellular growth of mice undergoing transverse aortic constriction (TAC) surgery. The different overexpression protocols such as adeno-associated virus-mediated Mettl3 overexpression and cardiomyocyte-specific transgenic Mettl3 overexpression may explain the discrepancy. In this study, we observed no changes in cardiac structure or function in conventional Mettl3-knockout heterozygous mice, while the electrophysiological property was significantly altered. Our finding indicates that changes in m^{6}A modification may be more prone to lead to electrophysiological disturbance than structural change in the heart.

Despite the critical role of Mettl3 in cell growth, cardiac homeostasis and hypertrophy, the role of Mettl3-mediated m^{6}A modification in mammalian heart electrophysiology has not been explored. In the present study, we found that I_{Ca-L} density was increased in ventricular myocytes of conventional Mettl3-knockout
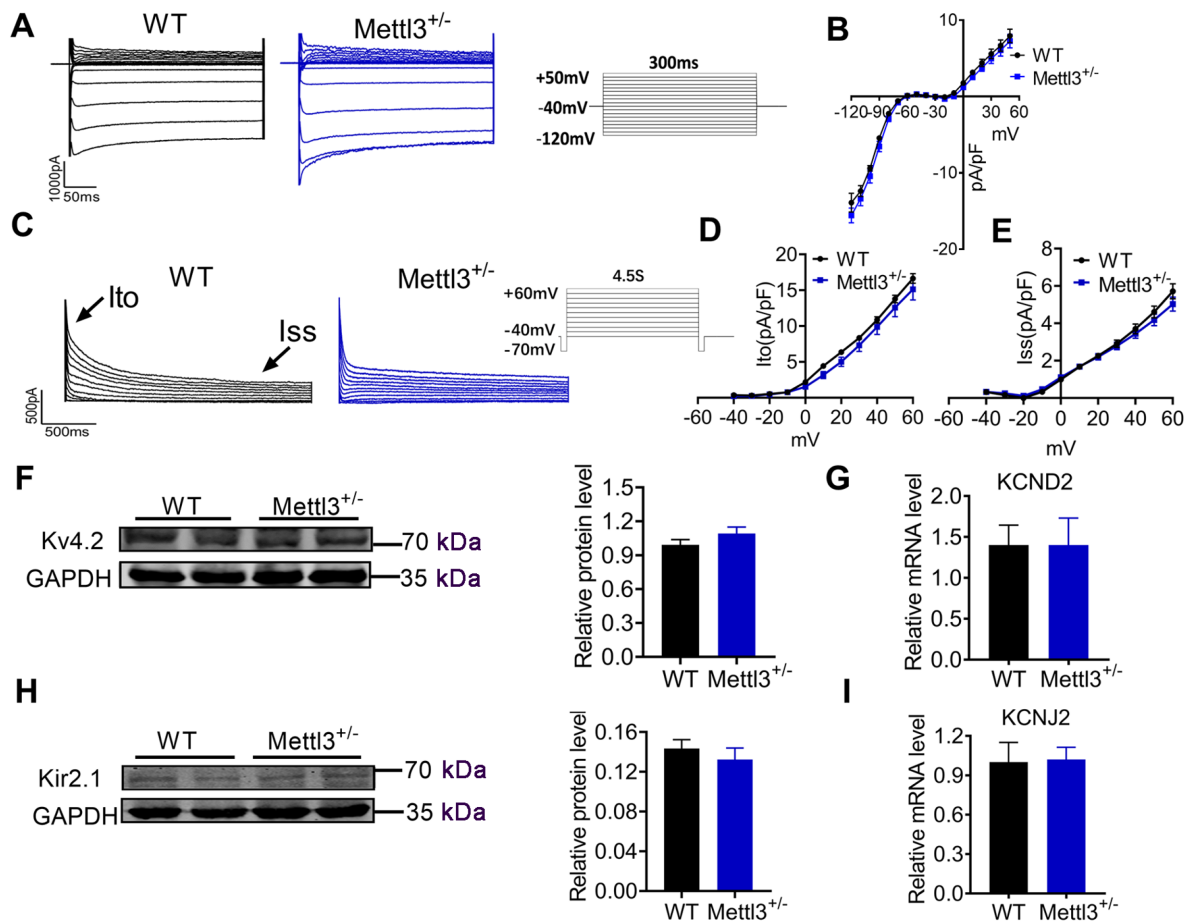
Figure 5. I_{k1} and I_{to} current in ventricular myocytes from WT and Mettl3$^{+/-}$ mice (A) Typical I_{k1} traces in WT and Mettl3$^{+/-}$ ventricular myocytes. (B) Current–voltage (I–V) relationships of I_{k1} in WT and Mettl3$^{+/-}$ ventricular myocytes (N = 18–20 cells). (C) Representative I_{to} traces in WT and Mettl3$^{+/-}$ ventricular myocytes. (D,E) Current–voltage (I–V) relationships of I_{to} and I_{ss} in WT and Mettl3$^{+/-}$ ventricular myocytes (n = 18–20 cells). Cells are from 5 mice. (F) Protein expression of Kv4.2 in WT and Mettl3$^{+/-}$ mice hearts. (G) mRNA expression of KCND2 in WT and Mettl3$^{+/-}$ mice hearts. (H) Protein expression of Kir2.1 in WT and Mettl3$^{+/-}$ mice hearts. (I) mRNA expression of KCNJ2 in WT and Mettl3$^{+/-}$ mice hearts. n = 3. Data are expressed as the mean ± SEM.

heterozygous mice, which underlies increased susceptibility to ventricular fibrillation. However, although we provide sufficient evidence for the increased I_{Ca-L} and prolonged action potential duration in Mettl3-knockout mice, we cannot exclude the possibility that other changes may also contribute to increased VF susceptibility. For example, we did not study the properties of all channels, ion transporters, and exchangers in Mettl3$^{+/-}$ ventricular myocytes. Because RMP and K channel expressions are different between neonates and adults, the balance between ion conductance including those involved in repolarization is thus quite different, for neonatal myocytes exhibit spontaneous activity, while adult myocytes do not. Therefore, using the data of neonatal cells to infer that adult mice is a shortcoming in our study. In addition, as the Mettl3$^{+/-}$ mice model is a global knockout model, the alterations exceeding the cardiac system may also participate in the regulation of Mettl3 on Cav1.2. A cardiac-specific knockout model would solve this problem.

In conclusion, deficiency of Mettl3 reduces the m^{6}A methylation level of *CACNA1C* mRNA, which leads to the increase of Cav1.2 protein and I_{Ca-L} currents and the consequent increased suscept-

ibility to ventricular arrhythmia. These findings indicate that m^{6}A methylation may represent a new mechanism in the regulation of cardiac ionic homeostasis and the development of arrhythmia.
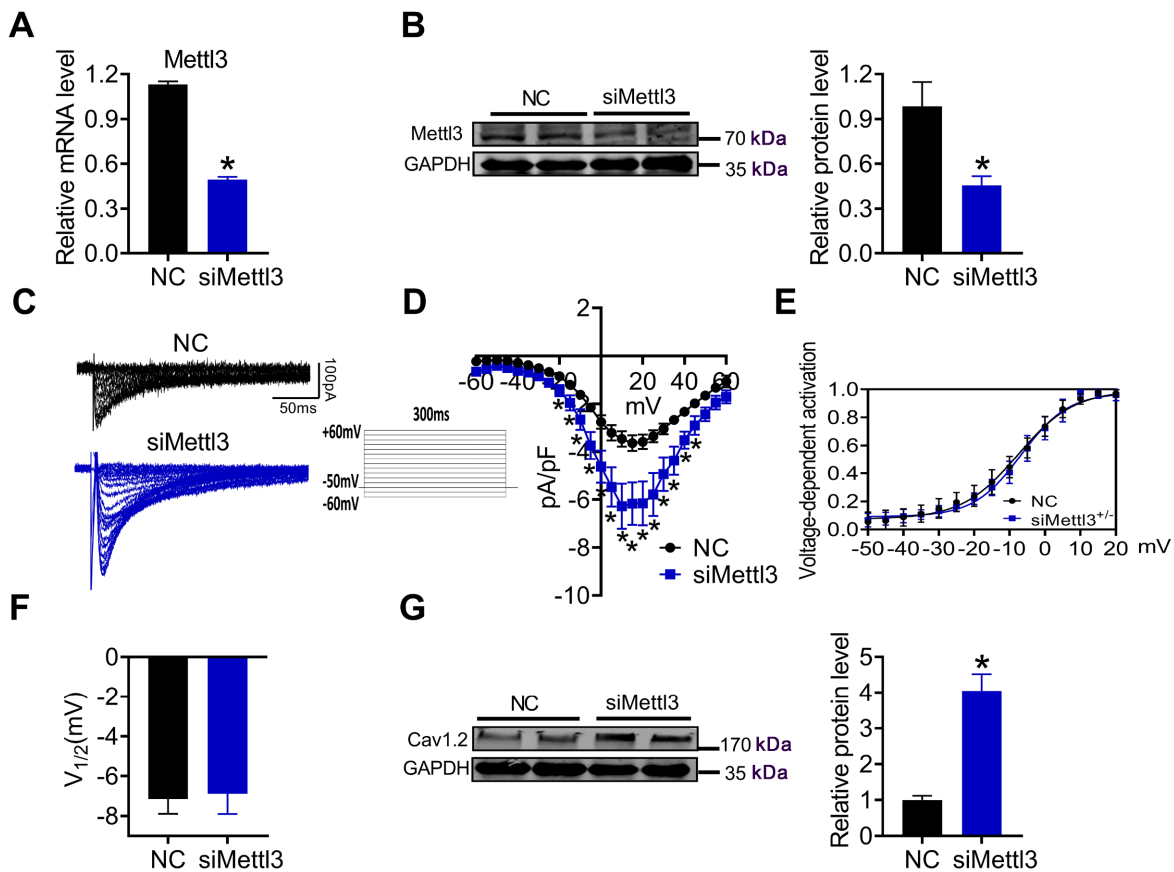
Conflict of Interest

The authors declare that they have no conflict of interest.

References

1. Wang CX, Cui GS, Liu X, Xu K, Wang M, Zhang XX, Jiang LY, *et al.* METTL3-mediated m^{6}A modification is required for cerebellar development. *PLoS Biol* 2018, 16: e2004880
2. Lin X, Chai G, Wu Y, Li J, Chen F, Liu J, Luo G, *et al.* RNA m^{6}A me-

Figure 6. Increase of I_{Ca-L} and upregulation of Cav1.2 in neonatal cardiomyocytes transfected with Mettl3 siRNA (A,B) Verification of Mettl3 down-regulation at both mRNA and protein levels in neonatal cardiomyocytes transfected with NC or Mettl3 siRNA (n = 3). (C) Representative traces of I_{Ca-L} in neonatal cardiomyocytes transfected with NC or Mettl3 siRNA. (D) Statistical analysis of the current density of I_{Ca-L}. (E) Voltage-dependent I_{Ca-L} activation. (F) Voltage for the half-maximal activation $V_{1/2}$. n = 10–12 cells. (G) The protein level of Cav1.2 in neonatal cardiomyocytes trans-fected with NC or Mettl3 siRNA (n = 3). Data are expressed as the mean ± SEM. *$P < 0.05$ vs WT by t-test.
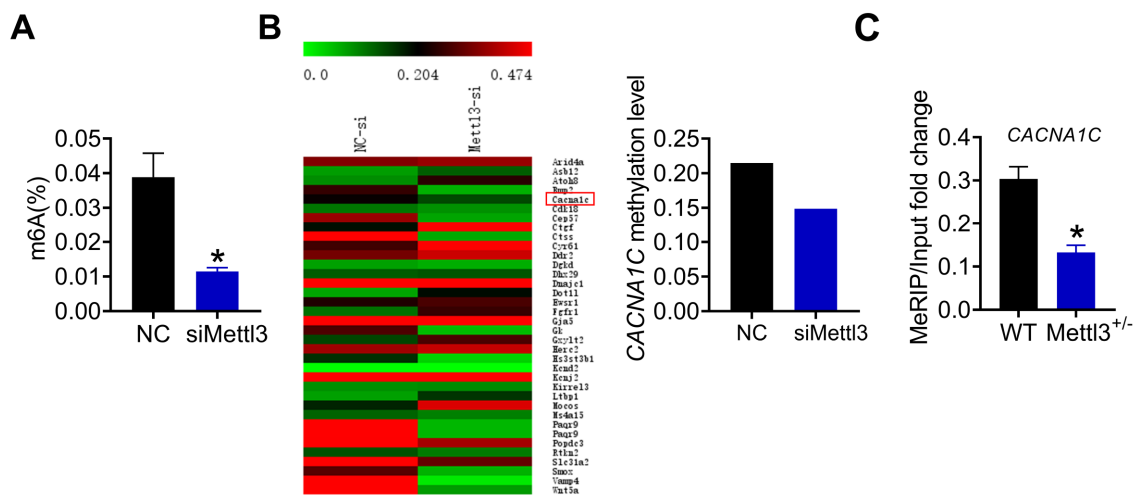
Figure 7. Decrease of *CACNA1C* m⁶A modification after Mettl3 deficiency (A) Percentage of m⁶A-methylated RNA in relation to unmodified adenosine as quantified by antibody-mediated m⁶A capture assay in NC and Mettl3-si neonatal mice cardiomyocytes. (B) m⁶A-mRNA epitran-scriptomic microarray was used to screen for differential mRNAs in Mettl3-knockdown mice cardiomyocytes. (C) MeRIP analysis followed by qRT-PCR was applied to assess the m⁶A modification of *CACNA1C* in WT and Mettl3⁺/⁻ mice. The enrichment of m⁶A in each group was calculated by m⁶A-IP/input.*$P < 0.05$ vs WT by t-tests.

thylation regulates the epithelial mesenchymal transition of cancer cells and translation of Snail. *Nat Commun* 2019, 10: 2065

3. Liu S, Zhuo L, Wang J, Zhang Q, Li Q, Li G, Yan L, *et al.* METTL3 plays multiple functions in biological processes. *Am J Cancer Res* 2020, 10: 1631–1646

4. Qin Y, Li L, Luo E, Hou J, Yan G, Wang D, Qiao Y, *et al.* Role of m⁶A RNA methylation in cardiovascular disease (Review). *Int J Mol Med* 2020, 46: 1958–1972

5. Wu S, Zhang S, Wu X, Zhou X. m⁶A RNA methylation in cardiovascular diseases. *Mol Ther* 2020, 28: 2111–2119

6. Wang Q, Chen C, Ding Q, Zhao Y, Wang Z, Chen J, Jiang Z, *et al.* METTL3-mediated m⁶A modification of HDGF mRNA promotes gastric cancer progression and has prognostic significance. *Gut* 2020, 69: 1193–1205

7. Jin D, Guo J, Wu Y, Du J, Yang L, Wang X, Di W, *et al.* m⁶A mRNA methylation initiated by METTL3 directly promotes YAP translation and increases YAP activity by regulating the MALAT1-miR-1914-3p-YAP axis to induce NSCLC drug resistance and metastasis. *J Hematol Oncol* 2019, 12: 135

8. Dorn LE, Lasman L, Chen J, Xu X, Hund TJ, Medvedovic M, Hanna JH, et al. The N⁶-methyladenosine mRNA methylase METTL3 controls cardiac homeostasis and hypertrophy. *Circulation* 2019, 139: 533–545

9. Song H, Feng X, Zhang H, Luo Y, Huang J, Lin M, Jin J, *et al.* METTL3 and ALKBH5 oppositely regulate m⁶A modification of *TFEB* mRNA, which dictates the fate of hypoxia/reoxygenation-treated cardiomyocytes. *Autophagy* 2019, 15: 1419–1437

10. Li T, Zhuang Y, Yang W, Xie Y, Shang W, Su S, Dong X, *et al.* Silencing of METTL3 attenuates cardiac fibrosis induced by myocardial infarction via inhibiting the activation of cardiac fibroblasts. *FASEB J* 2021, 35: e21162

11. Wang Y, Li C, Shi L, Chen X, Cui C, Huang J, Chen B, *et al.* Integrin β1D deficiency–mediated RyR2 dysfunction contributes to catecholamine-sensitive ventricular tachycardia in arrhythmogenic right ventricular cardiomyopathy. *Circulation* 2020, 141: 1477–1493

12. Li J, Xu C, Liu Y, Li Y, Du S, Zhang R, Sun Y, *et al.* Fibroblast growth factor 21 inhibited ischemic arrhythmias via targeting miR-143/EGR1 axis. *Basic Res Cardiol* 2020, 115: 9

13. Jin X, Jiang Y, Xue G, Yuan Y, Zhu H, Zhan L, Zhuang Y, *et al.* Increase of late sodium current contributes to enhanced susceptibility to atrial fibrillation in diabetic mice. *Eur J Pharmacol* 2019, 857: 172444

14. Chandra M, Escalante-Alcalde D, Bhuiyan MS, Orr AW, Kevil C, Morris AJ, Nam H, *et al.* Cardiac-specific inactivation of LPP3 in mice leads to myocardial dysfunction and heart failure. *Redox Biol* 2018, 14: 261–271

15. Zhang Y, Jiao L, Sun L, Li Y, Gao Y, Xu C, Shao Y, *et al.* LncRNA *ZFAS1* as a SERCA2a Inhibitor to Cause Intracellular Ca²⁺ Overload and Contractile Dysfunction in a Mouse Model of Myocardial Infarction. *Circ Res* 2018, 122: 1354–1368

16. Hedley PL, Jørgensen P, Schlamowitz S, Wangari R, Moolman-Smook J, Brink PA, Kanters JK, *et al.* The genetic basis of long QT and short QT syndromes: a mutation update. *Hum Mutat* 2009, 30: 1486–1511

17. Wit AL. Afterdepolarizations and triggered activity as a mechanism for clinical arrhythmias. *Pacing Clin Electrophysiol* 2018, 41: 883–896

18. Catterall WA. Structure and Regulation of Voltage-Gated Ca²⁺ Channels. *Annu Rev Cell Dev Biol* 2000, 16: 521–555

19. Song Z, Ko CY, Nivala M, Weiss JN, Qu Z. Calcium-voltage coupling in the genesis of early and delayed afterdepolarizations in cardiac myocytes. *Biophysl J* 2015, 108: 1908–1921

20. Bartos DC, Grandi E, Ripplinger CM. Ion Channels in the Heart. *Compr Physiol* 2015, 5: 1423-1464

21. Nuss HB, Kääb S, Kass DA, Tomaselli GF, Marbán E. Cellular basis of ventricular arrhythmias and abnormal automaticity in heart failure. *Am J Physiol-Heart Circulatory Physiol* 1999, 277: H80–H91

22. Fu Y, Dominissini D, Rechavi G, He C. Gene expression regulation mediated through reversible m6A RNA methylation. *Nat Rev Genet* 2014, 15: 293–306

23. Wang X, Zhao BS, Roundtree IA, Lu Z, Han D, Ma H, Weng X, *et al.* N6-methyladenosine modulates messenger RNA translation efficiency. *Cell* 2015, 161: 1388–1399

24. Dominissini D, Moshitch-Moshkovitz S, Schwartz S, Salmon-Divon M, Ungar L, Osenberg S, Cesarkas K, *et al.* Topology of the human and mouse m⁶A RNA methylomes revealed by m6A-seq. *Nature* 2012, 485: 201–206

25. Geula S, Moshitch-Moshkovitz S, Dominissini D, Mansour AAF, Kol N, Salmon-Divon M, Hershkovitz V, *et al.* m⁶A mRNA methylation facilitates resolution of naïve pluripotency toward differentiation. *Science* 2015, 347: 1002–1006

26. Fry NJ, Law BA, Ilkayeva OR, Holley CL, Mansfield KD. N⁶-methyladenosine is required for the hypoxic stabilization of specific mRNAs. *RNA* 2017, 23: 1444–1455

27. Choe J, Lin S, Zhang W, Liu Q, Wang L, Ramirez-Moya J, Du P, *et al.* mRNA circularization by METTL3–eIF3h enhances translation and promotes oncogenesis. *Nature* 2018, 561: 556–560

28. Kmietczyk V, Riechert E, Kalinski L, Boileau E, Malovrh E, Malone B, Gorska A, *et al.* m⁶ A-mRNA methylation regulates cardiac gene expression and cellular growth. *Life Sci Alliance* 2019, 2: e201800233